CRYSTAL Research&Technology
www.crt-journal.org

Synthesis and Improved Photoluminescent Properties and Stability of Bromine-Rich $CsPbBr_3$ Nanocrystals Via using CTAB as Additive

Shaohua Chi, Shuo Yang, Yansen Sun, Zhenyu Pang, Xiaoxu Sun, Lin Fan, Fengyou Wang, Xiaoyan Liu, Maobin Wei, Jinghai Yang, Nannan Yang,* and Lili Yang**

Although $CsPbBr_3$ nanocrystals (NCs) show excellent optoelectronic properties, their stability greatly limits their potential applications due to the ionicity. Stable bromine-rich $CsPbBr_3$ nanocrystals (NCs) are achieved by the thermal injection method, which includes adding cetyltrimethylammonium bromide (CTAB) to a cesium oleate precursor solution. The CTAB as a ligand provides strong binding to the NC surface to effectively passivate the surface defects, and most importantly helps to realize the formation of bromine-rich $CsPbBr_3$ NCs. The obtained bromine-rich $CsPbBr_3$ NCs show higher photoluminescence quantum yields (PLQYs) and enhanced moisture and UV illumination stability. These results provide a simple strategy to synthesize bromine-rich $CsPbBr_3$ NCs, which can be promising for integrating into the synthesize technique of perovskite optoelectronic devices.

1. Introduction

All-inorganic cesium halide lead perovskite nanocrystals ($CsPbX_3$, X = Cl, Br, I) has attracted significant attention owing to the tunable bandgap, narrow emission band, wide absorption band, high tolerance and high photoluminescence quantum yield, which becomes the next generation of potential materials for photoelectric devices. So far, $CsPbX_3$ perovskite has been widely utilized to fabricate solar cells and light-emitting diodes, which exhibits excellent performance. For instance, the power conversion efficiency (PCE) of optimized $CsPbI_{3-x}Br_x$ perovskite solar cells (PSCs) have reached 20.8% and $CsPbBr_3$ NC light emitting diodes (LEDs) have exhibited an external quantum efficiency (EQE) of 28.1%.[1,2] However, ionic nature, surface instability, and metastable structure of $CsPbX_3$ nanocrystals (NCs) lead to their degradation upon exposure to water, polar solvent, heat, and light irradiation, making them sensitive to environmental factors.[3,4]

Besides component control, surface modification or packaging has been utilized to enhance the stability of $CsPbX_3$ NCs. For example, partially or completely covering SiO_2 shell on $CsPbBr_3$ NCs can dramatically reduce its sensitivity to air, water, and light exposure. Although such a thick shell layer could effectively protect $CsPbBr_3$ NCs from the external environment, it would also hinder charge transfer within the devices.[5] As for another way of surface modification, the selection of capping ligands is critical to the final modification effect. The binding strength between these capping ligands and $CsPbX_3$ NCs have a great influence on the stability and optical properties.[6] Although Oleic (OA) and oleylamine (OLA) are traditionally required for the preparation process of $CsPbX_3$ NCs, they have a weak binding to the crystal surface, resulting in the easy decomposition of $CsPbX_3$ NCs. So far, the ligands with strong binding such as trioctylphosphine (TOP), oxide trioctylphosphine (TOPO), and alkylphosphonate have been widely adopted to replace the traditional capped ligand, which hinders the aggregation and decomposition of perovskite NCs, but cannot passivate the inherent defects within perovskite NCs.[7–9]According to previous reports, cetyltrimethylammonium bromide (CTAB) can be used as bromine source to prepare $CsPbBr_3$ perovskite quantum dots (PQDs) by water bath substitution method (instead of OLA) or room temperature solvent resistance method. The photoluminescence quantum yield (PLQY) of the synthesized $CsPbBr_3$ PODs was as high as 71%. Then, in order to improve the stability of PQDs, a protective layer was introduced into the synthesis of high stability

S. Chi, Y. Sun, Z. Pang, X. Sun
Changchun Institute of Optics
Fine Mechanics and Physics
Chinese Academy of Sciences
Changchun 130033, P. R. China
S. Chi, Y. Sun, Z. Pang, X. Sun
University of Chinese Academy of Sciences
Beijing 100049, P. R. China
S. Chi, Y. Sun, Z. Pang, X. Sun, L. Fan, F. Wang, X. Liu, M. Wei, J. Yang, L. Yang
Key Laboratory of Functional Materials Physics and Chemistry of the Ministry of Education
Jilin Normal University
Changchun 130103, P. R. China
E-mail: jhyang1@jlnu.edu.cn; llyang@jlnu.edu.cn
S. Yang
College of Science
Changchun University
Changchun 130022, P. R. China
N. Yang
College of Mechanical Engineering
Jilin Engineering Normal University
Changchun 130052, P. R. China
E-mail: yangnannan@jlenu.edu.cn

DOI: 10.1002/crat.202200051

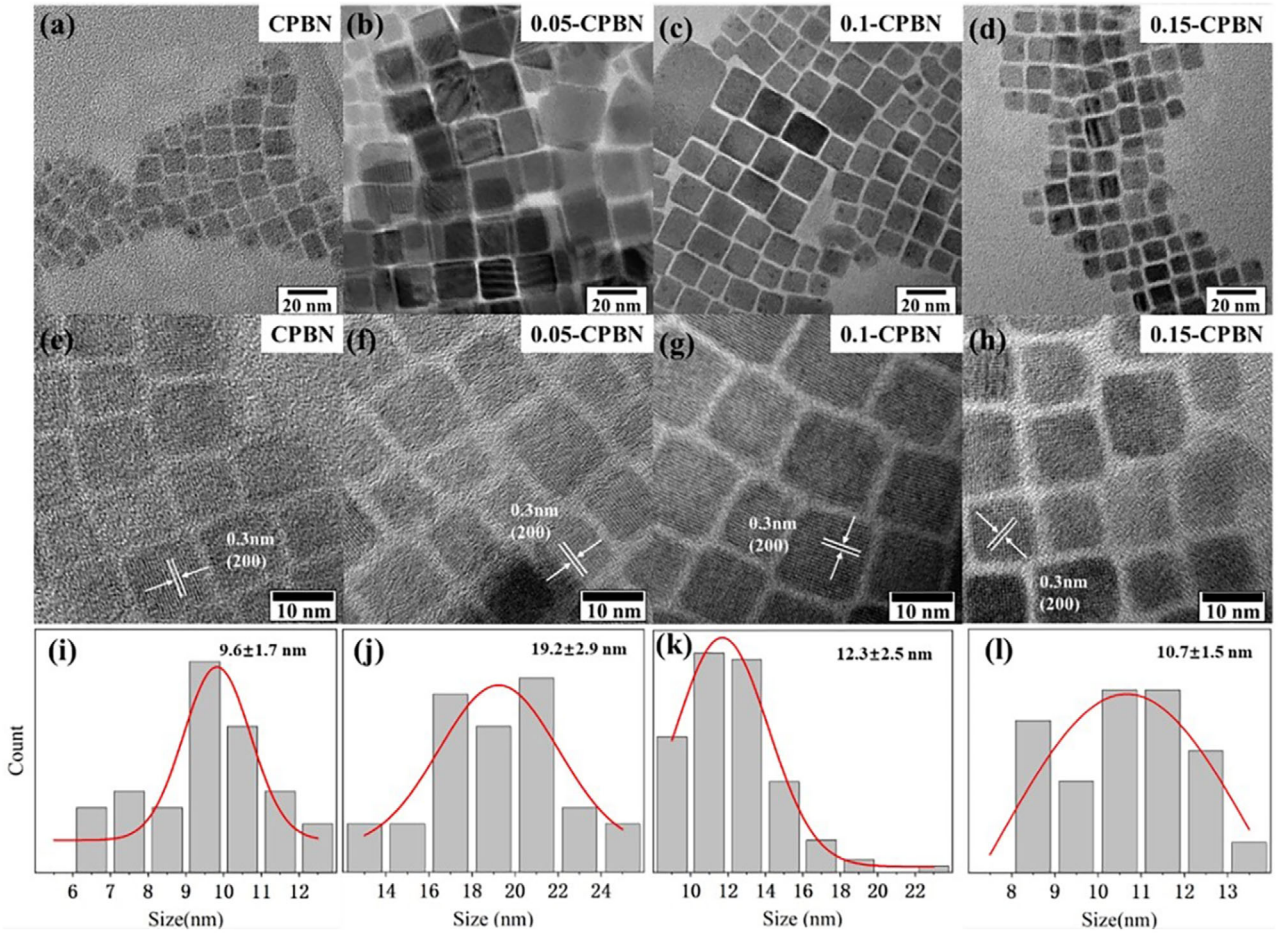

Figure 1. TEM images (20 nm scale bar and 10 nm scale bar) and grain size distributions (obtained from TEM images) of a,e,i) CPBN, b,f,j) 0.05-CPBN, c,g,k) 0.1-CPBN, and d,h,l) 0.15-CPBN.

quantum dots.[10,25] However, the formation of protective layer requires complex treatment and will reduce solubility or dispersion. Therefore, it is necessary to explore novel and simple introduction technique of multifunctional ligands to overcome both low PLQY and complex protective layer decorating process.

In this work, we combine the water bath heating method and surface engineering strategy together to develop a simple one-pot fabrication method to synthesize $CsPbBr_3$ NCs with high-quality and high PLQY, in which both CTAB and OLA will serve as passivator and protector to copassivate and protect $CsPbBr_3$ NCs. The reasons for selecting CTAB as additive are listed as follows: (1) CTA^+ has a strong affinity for negative ions and a shorter branched chain; (2) Since the surface of these NCs is terminated by halide and cesium ions, an ion-pair ligand can be an effective dual passivating agent; (3) Alkylammonium halide (mostly bromide) ion-pairs are more effective in surface passivating the inherent defects caused by halide vacancies. To reveal how CTAB passivate the defects and improve the environmental stability of $CsPbBr_3$ NCs, we studied the influence of amount of CTAB addition on the structure, optical properties, and stability of $CsPbBr_3$ NCs and reveal the corresponding modulation mechanism of CTAB in detail. As a result, the stability and crystal quality of $CsPbBr_3$ NCs have been successfully improved without other protective layer, and the PLQY is also enhanced up to 84%. We hope that our technology can bring new insights and help solve the inherent instability of tribromide perovskite materials and devices.

2. Results and Discussion

To optimize the synthesis procedure, we examined the effect of CTAB adding amount on the structure of $CsPbBr_3$ NCs. **Figure 1** shows the transmission electron microscopy (TEM), high-resolution transmission electron microscopy (HRTEM), and particle size distribution histograms images of as-synthesized CPBN, 0.05-CPBN, 0.1-CPBN, and 0.15-CPBN. Obviously, the as-synthesized control CPBN exhibits cubic shape with an average diameter of 9.6 nm. The corresponding HRTEM image exhibits a lattice plane distance of 0.3 nm, corresponding to the (200) plane of the monoclinic-phase $CsPbBr_3$ (**Figure 2**).[11–13] Meanwhile, some dark spots appeared on the $CsPbBr_3$ NCs, which are usually assigned to unreacted $PbBr_2$ particles according to previous reports.[14] After introducing 0.05 mmol CTAB, the $CsPbBr_3$ NCs tend to self-assemble into "face-to-face" stacking nanosheets and those dark spots were totally disappeared, indicating the high crystal quality of 0.05-CPBN had been achieved. Meanwhile, the

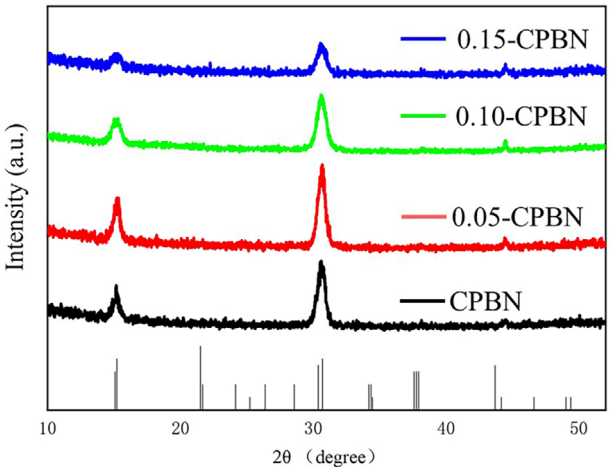

Figure 2. XRD patterns of CPBN, 0.05-CPBN, 0.1-CPBN, and 0.15-CPBN.

average diameter of $CsPbBr_3$ NCs also increased up to 19.2 nm. One of reason is that the CTAB is a highly active surface ligand, the surface activity of $CsPbBr_3$ NCs turns higher, which leads to the acceleration of crystal growth rate and prompt the achievement of $CsPbBr_3$ NCs with larger size.[15] In addition, the unreacted $PbBr_2$ exists in the solution of oleic acid or ammonium ion complex. According to the following equation[16]

$$(C_{17}H_{33}COO)_2Pb + 2C_{18}H_{35}NH_2Br \rightarrow PbBr_2 \downarrow + 2(C_{17}H_{33}COO)^-(C_{18}H_{35}NH_2)^+ \quad (1)$$

the $PbBr_2$ would precipitate out, while oleate and ammonium oleate form ion pairs. The disappearance of lead bromide black spots proves that CTAB can improve the surface activity of nanocrystals. The addition of appropriate amount of CTAB can improve the reaction activity of the precursor solution and then increase the reaction rate and promote the production of nanocrystals. This is beneficial to the complete crystallization of $CsPbBr_3$ NCs, which can effectively inhibit the occurrence of the above reactions and eliminate the black spots. Interestingly, with further increasing the adding amount of CTAB up to 0.1 and 0.15 mmol, the dark particles appeared and average diameter decreased again. It is attributed to the fact that high ligand concentration will reduce the reaction activity of the precursor solution and provide a relatively inert environment, and lead to the decrease of nanocrystal growth rate.[17] In addition, CTAB as an Alkyl quaternary ammonium salt (QAHs) is a well-known cationic surfactant. For these molecules, the high polar nitrogen part usually makes them show poor solubility in nonpolar or weak polar solvents such as toluene and octadecene (ODE). This is also the reason why only a small amount of CTAB is needed in the synthesis of $CsPbBr_3$ NCs.

The X-ray diffraction (XRD) patterns were performed to analyze the composition and phase structure of the samples. As shown in Figure 2, all as-synthesized $CsPbBr_3$ NCs exhibit three strong diffraction peaks at 15.2°, 30.6°, and 44.1°, which can be assigned to the (100), (200), and (220) plane according to the JCPDS #18-0364, confirming the formation of perovskite structure with monoclinic phase.[18,19] Obviously, the introduction of CTAB did not significantly affect the crystal structure of $CsPbBr_3$ NCs. As for all the $CsPbBr_3$ NCs modified by CTAB, the intensity of (200) diffraction peak of 0.05-CPBN turned to be strongest, indicating high crystal quality has been obtained due to the defect passivation. However, with further increasing the amount of CTAB, the intensity gradually reduced, indicating the crystal quality turned poor again.

Here we propose a possible influence mechanism of CTAB on the growth of CPBN. It is well known that cubic $CsPbBr_3$ consists of periodically arranged Pb–Br octahedrons and isolated cesium ions.[20] It is worth noting that the band edge is formed by Br 4p and Pb 6p orbitals, while the interaction of Cs ions is very weak and makes little contribution to the electronic structure of the band edge.[21] In other words, the recombination of excitons is limited to $PbX6^{4-}$ octahedron, and only the changes of surface Pb and Br states affect the optical properties. Since there are only dozens of unit cells due to the small size of $CsPbBr_3$ and the formation energy of interstitial and antilattice defects is very high, the internal defects are negligible compared with surface defects.[22,23] This greatly simplifies the problem so that we can consider that there are only two kinds of vacancy defects (V_{Br} and V_{Pb}) on the surface. As shown in **Figure 3**, when there is V_{Pb} on the surface, the entire structural unit loses the edge of the Pb–Br octahedron, but the other structural units remain unchanged. The bromine ion in halogenated alkylamine will fill the empty angle of PbX_{6-y} octahedron, and the amine cation will bind to the hanging bond of Br ion. In addition, when there are V_{Br} defects, lead ions will be exposed and stabilized by oleate.

To prove above proposal, Fourier-transform infrared (FTIR) spectroscopy was conducted to analyze the ligand attachment to the NC surface. As can be seen from **Figure 4**, for all samples, the absorption at 1605 and 1406 cm^{-1} is attributed to an asymmetric vibration and a symmetrical stretching vibration of the carboxylic acid group, indicating that oleic acid anions are complexed on the surface of CsPbBr3 NCs.[24] In comparison with the spectrum of CPBN, the spectra of CTAB-modified $CsPbBr_3$ NCs exhibit stronger signal at 2850 and 2920 cm^{-1}, which is respectively corresponding to the CH_2 and CH_3 symmetric and asymmetric stretching vibrations of OA and OLA ligands, indicating the addition of CTAB does not counteract the contribution of OA and OLA to nanocrystals. Meanwhile, the peak corresponding to $C–N^+$ tensile vibration can be observed at 907 and 960 cm^{-1}.[26] These signals are the typical absorption bands for CTAB, further indicating the both of CTAB and OA/OLA play a double passivation effect on nanocrystals. In addition, the strong signal at 1635 cm^{-1} of the $CsPbBr_3$ NCs and CTAB modified $CsPbBr_3$ NCs can be attributed to the asymmetric NH_3^+ deformation.[18,25]

The UV–vis absorption spectra, PL spectra and photoluminescence yields (PLQYs) of CPBN and 0.05-CPBN are shown in **Figure 5**. Both CPBN and 0.05-CPBN show a strong emission band under the excitation of 365 nm, and the maximum emission intensity at 515 nm. Obviously, the introduction of CTAB did not significantly change its emission peak position, indicating the addition of CTAB did not bring great change in the perovskite structure. Meanwhile, the full width at half maximum (FWHM) decreased from 20 to 18 nm and the fluorescence intensity at 515 nm were enhanced after introducing CTAB, which further proved that the surface trap state in 0.05-CPBN had been effectively passivated. In addition, the $CsPbBr_3$ nanocrystalline

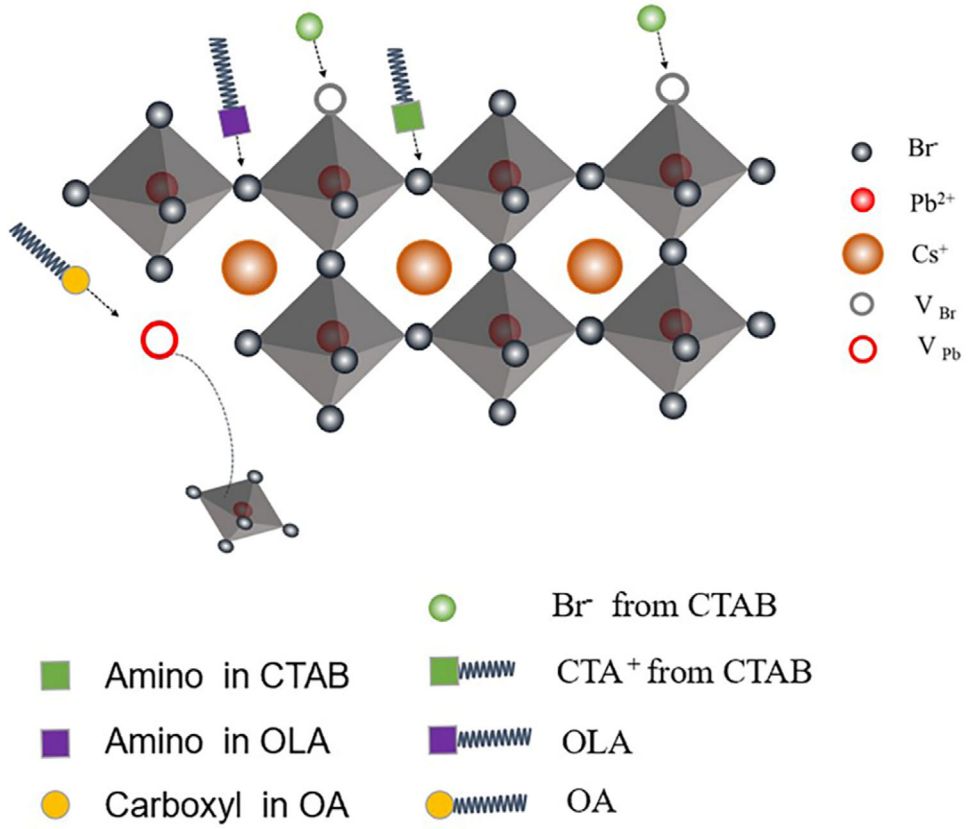

Figure 3. Schematic depiction of surface passivation.

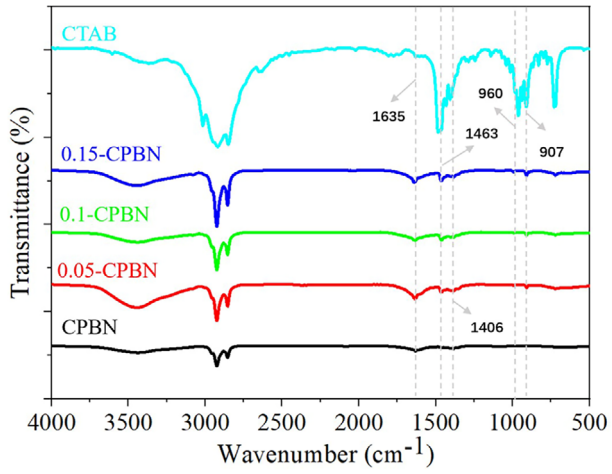

Figure 4. FTIR transmission spectra of the CPBN, 0.05-CPBN, 0.1-CPBN, and 0.15-CPBN prepared from different adding amount of CTAB.

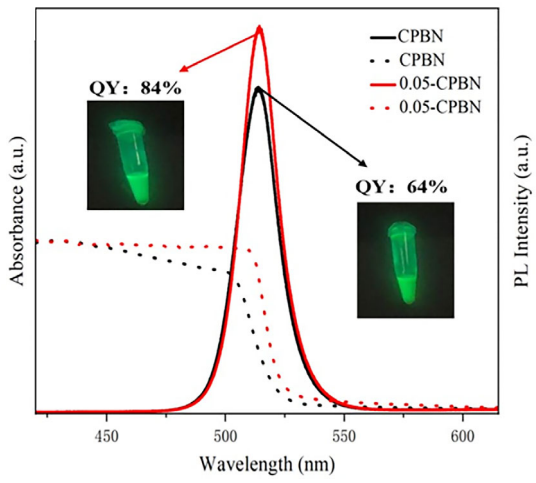

Figure 5. UV–vis absorption spectrum and PL emission spectrum of CPBN and 0.05-CPBN. The insets show photographs of the corresponding samples under excitation of 365 nm UV light.

solution emits bright green when excited by 365 nm, and the quantum yield increases from 64% to 84%. According to the literature, $PbBr_2$ particles are other ways to cause nonradiative attenuation, so the elimination of $PbBr_2$ particles may be another factor to lead to the PLQY enhancement.[13,15,29]

Figure 6 presents the time-resolved PL spectra of CPBN and 0.05-CPBN. The average PL lifetime were estimated using Equation 2

$$\tau_{av} = \frac{\sum_i A_i \tau_i^2}{\sum_i A_i \tau_i} \quad (2)$$

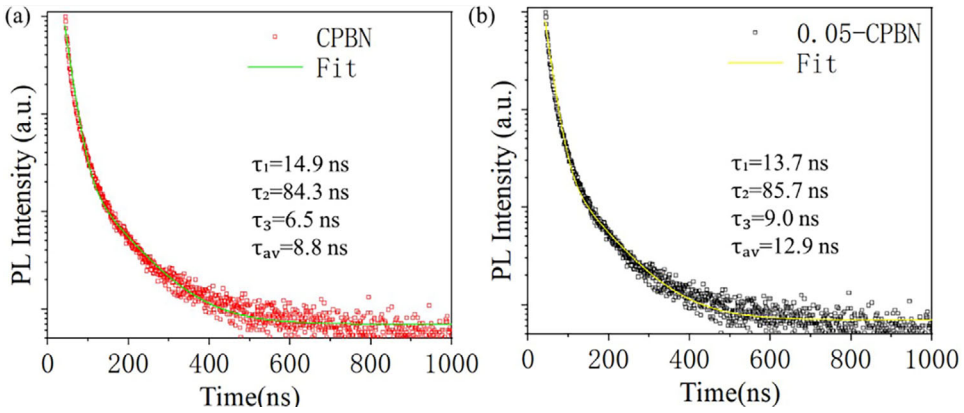

Figure 6. Time-resolved PL for a) CPBN and b) 0.05-CPBN solutions.

Table 1. Lifetimes and associated fraction amplitudes resulting from a biexponential fit to the PL decay transients for QDs-control and QDs-passivated samples.

Sample	A_1 [%]	τ_1 [ns]	A_2 [%]	τ_2 [ns]	A_3 [%]	τ_3 [ns]	τ_{ave} [ns]
CPBN	10.08	6.46	13.13	14.89	0.052	84.31	8.80
0.05-CPBN	10.80	8.96	13.83	13.73	0.037	85.74	12.9

Table 2. Atomic percentages from quantitative XPS analysis.

Atomic %	C	Cs	Pb	Br
CPBN	81.98	0.35	0.28	1.09
0.05-CPBN	74.46	0.25	0.22	0.87

where A_i and τ_i are used to fit the weight and time components of the exponential function of the PL decay curve. As shown in Figure 6, the PL decay of 0.05-CPBN is also slower than that of CPBN, and the average lifetimes increased from 8.8 to 12.9 ns, suggesting defect passivation and less nonradiative recombination via defect states happened in 0.05-CPBN, which is consistent with the results of Figure 5. The PL decay transients of OA/OLA-capped $CsPbBr_3$ NCs and CTAB-capped $CsPbBr_3$ NCs can be best described by a triple exponential decay function. The fitted lifetime of τ_1, τ_2, and τ_3 is corresponding to the intrinsic exciton relaxation, the interaction between excitons and phonons, and the interaction between excitons and defects, respectively.[27–29,31] The fitted lifetime of τ_1, τ_2, and τ_3 in CPBN is 6.5, 14.9, and 84.3 ns, respectively (**Table 1**), respectively. And the fitted lifetime of τ_1, τ_2, and τ_3 in 0.05-CPBN is 9.0, 13.7, and 85.7 ns, respectively. The average lifetime (τ_{av}) is then calculated to be 8.8 and 12.9 ns for CPBN and 0.05-CPBN, respectively. It is well known that the surface defects on $CsPbBr_3$ nanocrystals will serve as nonradiative recombination channel in addition to light emission, which will shorten the attenuation lifetime of PL and reduce PLQY.[32,33] Compared with the unmodified quantum dots, CTAB-CQDs shows a longer effective fluorescence lifetime, which indicates that the nonradiative recombination can be successfully suppressed by surface modification.

To further explore the passivated principles of CTAB, we performed X-ray photoelectron spectroscopy (XPS) measurement on CPBN and 0.05-CPBN samples. **Figure 7**a presented the survey XPS spectra of both samples. Obviously, the elements of Cs, Pb, Br, C, and O existed in both samples. Figure 7b shows that the binding energy of Cs^+ is relatively stable before and after CTAB passivation, indicating that the interaction between Cs^+ and surface ligands in perovskite crystals is not significant. In Figure 7c, the peaks with binding energies of 143 and 143.3 eV belong to the Pb 4f 5/2 of CPBN and 0.05-CPBN, respectively, and the peaks of 138 and 138.3 eV belong to the Pb 4f 7/2 of CPBN and 0.05-CPBN, respectively.[4] Similarly, in Figure 7d the peaks with binding energies of 69 and 69.3 eV are attributed to Br 3d 3/2 of CPBN and 0.05-CPBN, respectively, and the peaks of binding energies of 68 and 68.3 eV are attributed to Br 3d 5/2 of CPBN and 0.05-CPBN, respectively.[34] As for 0.05-CPBN, a shift to the larger binding energy appears for Pb 4f and Br 3d XPS spectra in comparison with those of the CPBN. Such shift indicated the binding between Pb and Br in 0.05-CPBN turned stronger due to the CTAB modification, which results in the improved PLQYs. Meanwhile, according to the quantitative XPS results (**Table 2**), the composition ratio of CPBN is Cs:Pb:Br = 1:0.8:3 and the corresponding ratio of 0.05-CPBN is Cs:Pb:Br = 1:0.8:3.4, indicating that the addition of CTAB ligands prevents the occurrence of halide defects in the 0.05-CPBN and leads to the formation of Br-rich NCs. According to the previous reports, the bromide ion-enriched surface of $CsPbBr_3$ NCs has a role in self-passivation to enhance photoluminescence properties, which is also consistent with our results.[35,36]

The surface defects and weak ligands–NCs interaction are the key factors to result in the instability and degradation of the $CsPbBr_3$ NCs in ambient conditions.[3,37–40] In order to verify whether the surface passivation of CTAB in our case could improve the stability or not, the corresponding time and moisture-dependent photostability were studied. As shown in **Figure 8**, the PL intensity of CPBN dropped to 39% of its initial value under UV exposure for 6 h, while the PL intensity of 0.05-CPBN remained over 90%. We believed that such better photostability of 0.05-CPBN was originated from the stable ligands anchored by the CTAB. In detail, as for perovskite NCs, the vacancies defects dominate their surface properties. After we used CTAB to modify CPBN, since CTA^+ has a strong affinity for negatively charged

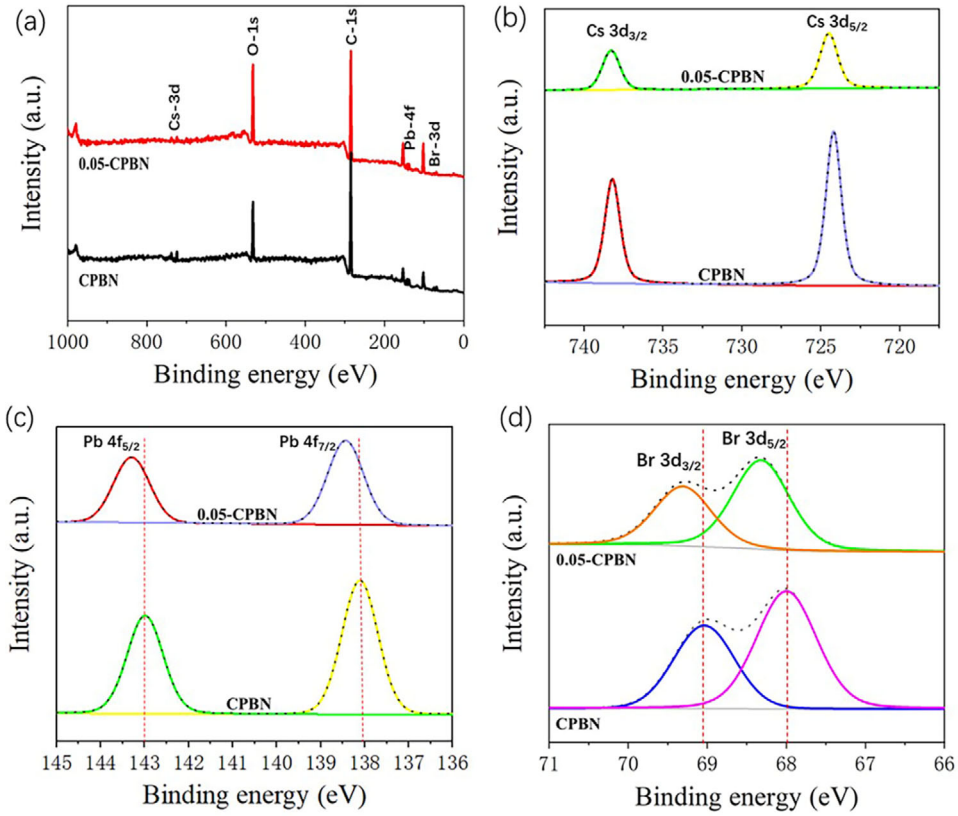

Figure 7. The X-ray photoelectron spectroscopy (XPS) of a) CPBN and 0.05-CPBN, b–d) the high-resolution XPS analysis corresponding to Cs^+ 3d, Pb^{2+} 4f, and Br^- 2p, respectively.

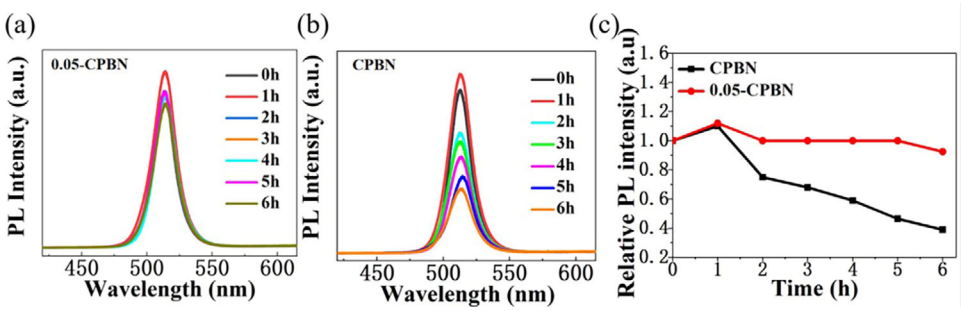

Figure 8. PL emission spectrum of a) 0.05-CPBN and b) CPBN; Normalized PL emission intensity of c) CPBN and 0.05-CPBN: solutions after different irradiation times with a 28 W (365 nm) UV lamp.

surface sites, the OA/OLA ligands separated from the surface of quantum dots are replaced by CTA^+, which helped to form the Br-rich $CsPbBr_3$ NCs and finally enhanced the long-term optical stability.

In addition, all samples showed enhanced luminescence after being exposed to UV light for 1 h. The increase in fluorescence intensity after exposure to ultraviolet light is often referred to as "light activation," also known as light enhancement. This pathway includes photoinduced rearrangement of surfactant molecules, which stabilize/passivate the holes on the surface of NCs, resulting in enhanced luminescence.[30,41] When CPBN and 0.05-CPBN were immersed in water with vigorous stirring, after soaking ultraviolet irradiation for 90 min, the fluorescence intensity of CPBN decreased sharply to 31%, while 0.05-CPBN maintained 91% of the original integral emission intensity, suggesting the hydrophobic nature of $CsPbBr_3$ NCs becomes stronger due to the passivation with the CTA^+ (**Figure 9**). These results indicate that the photostability and water stability of $CsPbBr_3$ NCs after CTAB passivation have been improved.

3. Conclusion

In summary, we developed a simple CTAB additive method to synthesize bromine-rich $CsPbBr_3$ NCs with enhanced

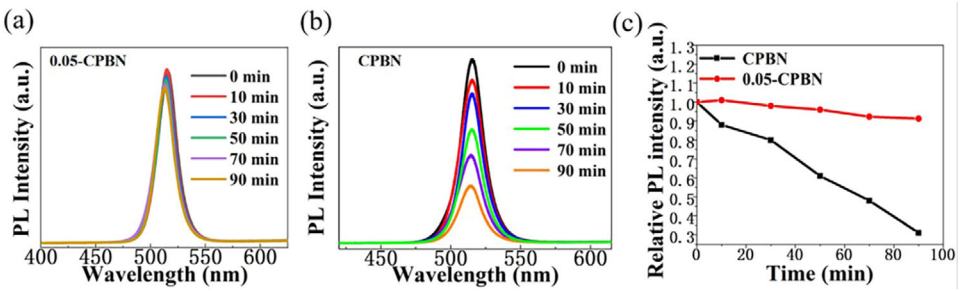

Figure 9. Time-dependent PL emission spectra under UV light of a) 0.05-CPBN and b) CPBN; Normalized PL emission intensity of c) CPBN and 0.05-CPBN: solutions with water in a 1:1 volume ratio.

photoluminescent properties and environmental stability (moisture and UV illumination). In comparison with the traditional OA and OLA capped NCs, the crystal quality, PLQY and the stability of monodispersed CTAB-capped bromine-rich $CsPbBr_3$ NCs have been enhanced. The PLQY of $CsPbBr_3$ NCs prepared by adding 0.05 mmol CTAB reached up to 84%, and it retained original PL intensity for at least 6 h under the ultraviolet irradiation. The improved PLQY and stability can be attributed to the CTAB ligands bound strongly to the surface of NCs, resulting in the effective passivation of surface defects and even more importantly the formation of a bromine-rich surface. These results provide a simple strategy to synthesize $CsPbBr_3$ NCs with environmental stability and high PLQYs, suggesting a broad prospect in optoelectronic applications.

4. Experimental Section

Materials: Cesium carbonate (Cs_2CO_3; 99.99%), octadecene (ODE; 90%), oleic acid (OA; 99%), oleylamine (OLA; 90%), hexadecyl trimethyl ammonium bromide (CTAB; 99%), lead bromide ($PbBr_2$; 99.99%), normal hexane. During use, all reagents were not further purified.

Synthesis of OA/OLA-CsPbBr3 NCs: First, the Cs_2CO_3 (0.22 g), OA (0.65 mL), and 10 mL ODE were mixed and put into a 100 mL three neck round-bottom flask to prepare the cesium oleate precursor. The mixture was desiccated under vacuum at 120 °C for 1 h, then heated up to 150 °C and stirred for 20 min under N_2 flow, till all Cs_2CO_3 was completely dissolved. ODE (5 mL), $PbBr_2$ (0.052 g), OA (0.5 mL), and OLA (0.5 ml) were mixed and stirred under vacuum at 120 °C for 1 h to prepare the Pb precursor. The Pb precursor was then heated to 170 °C, hot Cesium oleate solution (0.4 mL) was rapidly injected for 5 s and then the $CsPbBr_3$ perovskites solution was immediately cooled by ice-water bath. Then the cooled crude solution was centrifuged at 7500 rpm for 4 min. The supernatant was discarded and the particles were dispersed in normal hexane after centrifugation.

Synthesis of CTAB-Capped $CsPbBr_3$ NCs: The Cs_2CO_3 (0.22 g), OA (0.65 mL), CTAB (X mmol, X = 0.05, 0.1, 0.15) were mixed in 10 mL ODE in a 100 mL three-neck round bottom flask to prepare the cesium oleate precursor. The mixture was desiccated under vacuum at 120 °C for 1 h, then heated up to 150 °C and stirred for 20 min under N_2 flow, till a clear solution was obtained. It is worth noting that Cs-oleate precipitates out of ODE at room temperature, so preheating over 100 °C is needed to make it soluble before applying. Second, to prepare Pb-precursor solution, the $PbBr_2$ (0.052 g) was mixed with ODE (5 mL), OA (0.5 mL), and OLA (0.5 mL), loaded into 50 mL 3-neck flask, and degassed at 120 °C for 1 h under vacuum. The mixed solution was heated up to 170 °C. Finally, to synthesize the $CsPbBr_3$ NCs, the hot Cs-oleate solution (0.4 mL) was rapidly injected and stirred for 5 s at that temperature. The solution of CTAB capped $CsPbBr_3$ perovskites was cooled by ice-water bath immediately. Then the cooled crude solution was centrifuged at 7500 rpm for 4 min. The supernatant was discarded and the particles were dispersed in normal hexane after centrifugation. ($CsPbBr_3$ NCs capped with x mmol CTAB and OA/OLA-$CsPbBr_3$ NCs are named x-CPBN and CPBN).

Characterization: TEM and HRTEM images were taken on JEM-2100 electron microscope equipped. XRD patterns were obtained by using a Rigaku D/max-2500 X-ray powder diffractometer with a Cu Ka source. The step size (2θ) is 0.02°. UV–vis absorption spectra were recorded on a UV-3600 PC UV–vis spectrophotometer. Photoluminescence quantum yields (PLQYs) were measured using an Otsuka QE-2000 with an integrating sphere. The PLQYs were measured under the excitation of 365 nm UV light. Steady-state photoluminescence spectra (PL) were collected from a FluorologoiHR 320 Horiba Jobin Yvon spectrofluorimeter. Time-resolved PL measurements (TRPL) measurements were performed on a Horiba Jobin Yvon Fluorolog-3 fluorescence lifetime spectrometer. XPS measurements were performed by an ESCALab220i-XL electron spectrometer from VG Scientific. FTIR spectra were recorded using a Bruker Vertex 70 spectrophotometer in KBr pellets.

Acknowledgements

The authors would like to acknowledge financial support for this work from National Nature Science Foundation of China (Grant No. 61775081), the 13th Five-year Program for Science and Technology of Education Department of Jilin Province (Grant No. JJKH20200179KJ).

Conflict of Interest

The authors declare no conflict of interest.

Data Availability Statement

The data that support the findings of this study are available on request from the corresponding author. The data are not publicly available due to privacy or ethical restrictions.

Keywords

defect passivation, perovsktie nanocrystals, photoluminescence quantum yields (PLQYs), stability

Received: March 6, 2022
Revised: May 14, 2022
Published online: June 15, 2022

[1] Z. Liu, W. D. Qiu, X. M. Peng, G. W. Sun, X. Y. Liu, D. H. Liu, Z. C. Li, F. R. He, C. Y. Shen, Q. Gu, F. L. Ma, L. Yip, L. T. Hou, Z. J. Qi, S. J. Su, *Adv. Mater.* **2021**, *33*, 2103268.

[2] X. J. Gu, W. C. Xiang, Q. W. Tian, S. Z. Liu, *Angew. Chem., Int. Ed.* **2021**, *60*, 23164.
[3] N. Hao, J. W. Lu, Z. Dai, J. Qian, J. D. Zhang, Y. S. Guo, K. Wang, *Electrochem. Commun.* **2019**, *108*, 106559.
[4] K. K. Liu, Q. Liu, D. W. Yang, Y. C. Liang, L. Z. Sui, J. Y. Wei, G. W. Xue, W. B. Zhao, X. Y. Wu, L. Dong, C. X. Shan, *Light: Sci. Appl.* **2020**, *9*, 44.
[5] Q. G. Zhang, B. Wang, W. L. Zheng, L. Kong, Q. Wan, C. Y. Zhang, Z. C. Li, X. Y. Cao, M. M. Liu, L. Li, *Nat. Commun.* **2020**, *11*, 31.
[6] M. Lu, J. Guo, S. Q. Sun, P. Lu, X. Y. Zhang, Z. F. Shi, W. W. Yu, Y. Zhang, *Chem. Eng. J.* **2021**, *404*, 126563.
[7] S. Seth, T. Ahmed, A. Samanta, *J. Phys. Chem. Lett.* **2018**, *9*, 7007.
[8] J. De Roo, M. Ibanez, P. Geiregat, G. Nedelcu, W. Walravens, J. Maes, J. C. Martins, I. Van Driessche, M. V. Koyalenko, Z. Hens, *ACS Nano* **2016**, *10*, 2071.
[9] M. I. Bodnarchuk, S. C. Boehme, S. ten Brinck, C. Bernasconi, Y. Shynkarenko, F. Krieg, R. Widmer, B. Aeschlimann, D. Gunther, M. V. Kovalenko, I. Infante, *ACS Energy Lett.* **2019**, *4*, 63.
[10] J. Zhou, H. Lin, Y. Yu, S. Zuo, B. Li, J. Liu, *Chem. - Eur. J.* **2020**, *26*, 10528.
[11] T. Kosugi, Y. Iso, T. Isobe, *Chem. Lett.* **2019**, *48*, 349.
[12] Y. Wei, K. Li, Z. Cheng, M. Liu, H. Xiao, P. Dang, S. Liang, Z. Wu, H. Lian, J. Lin, *Adv. Mater.* **2019**, *31*, 1807592.
[13] T. Xuan, X. Yang, S. Lou, J. Huang, Y. Liu, J. Yu, H. Li, K. L. Wong, C. Wang, J. Wang, *Nanoscale* **2017**, *9*, 15286.
[14] M. A. Uddin, J. K. Mobley, A. A. Masud, T. Liu, R. L. Calabro, D. Y. Kim, C. I. Richards, K. R. Graham, *J. Phys. Chem. C* **2019**, *123*, 18103.
[15] Y. H. Huang, W. L. Luan, M. K. Liu, L. Turyanska, *J. Mater. Chem. C* **2020**, *8*, 2381.
[16] M. Zhang, H. B. Li, Q. Jing, Z. D. Lu, P. Wang, *Crystals* **2018**, *8*, 2.
[17] Z. H. Zhu, Y. Wu, Y. Shen, J. H. Tan, D. Shen, M. F. Lo, M. L. Li, Y. Yuan, J. X. Tang, W. J. Zhang, S. W. Tsang, Z. Q. Guan, C. S. Lee, *Chem. Mater.* **2021**, *33*, 4154.
[18] C. Zheng, C. Bi, F. Huang, D. Binks, J. Tian, *ACS Appl. Mater. Interfaces* **2019**, *11*, 25410.
[19] X. Zhang, X. Bai, H. Wu, X. Zhang, C. Sun, Y. Zhang, W. Zhang, W. Zheng, W. W. Yu, A. L. Rogach, *Angew. Chem., Int. Ed.* **2018**, *57*, 3337.
[20] T. Peyronel, K. J. Quirk, S. C. Wang, T. G. Tiecke, *Optica* **2016**, *3*, 787.
[21] A. Filippetti, A. Mattoni, *Phys. Rev. B* **2014**, *89*, 125203.
[22] Yang, X. L.i, Y. Wu, C. Wei, Z. Qin, C. Zhang, Z. Sun, Y. Li, Y. Wang, H. Zeng, *Adv. Opt. Mater.* **2019**, *7*, 1900276.
[23] J. Kang, L. W. Wang, *Phys. Chem. Chem. Phys.* **2017**, *8*, 489.
[24] J. Pan, L. N. Quan, Y. Zhao, W. Peng, B. Murali, S. P. Sarmah, M. Yuan, L. Sinatra, N. M. Alyami, J. Liu, E. Yassitepe, Z. Yang, O. Voznyy, R. Comin, M. N. Hedhili, O. F. Mohammed, Z. H. Lu, D. H. Kim, E. H. Sargent, O. M. Bakr, *Adv. Mater.* **2016**, *28*, 8718.
[25] L. J. Ruan, B. Tang, Y. Ma, *J. Phys. Chem. C* **2019**, *123*, 11959.
[26] Y. Cai, L. Wang, T. Zhou, P. Zheng, Y. Li, R. J. Xie, *Nanoscale* **2018**, *10*, 21441.
[27] S. Cho, S. Kim, J. Kim, Y. Jo, I. Ryu, S. Hong, J. J. Lee, S. Cha, E. B. Nam, S. U. Lee, S. K. Noh, H. Kim, J. Kwak, H. Im, *Light: Sci. Appl.* **2020**, *9*, 156.
[28] Z. Liang, S. Zhao, Z. Xu, B. Qiao, P. Song, D. Gao, X. Xu, *ACS Appl. Mater. Interfaces* **2016**, *8*, 28824.
[29] I. D. Stoev, B. Seelbinder, E. Erben, N. Maghelli, M. Kreysing, *eLight* **2021**, *1*, 7.
[30] D. Lee, S. So, G. Hu, M. Kim, T. Badloe, H. Cho, J. Kim, H. Kim, C.-W. Qiu, J. Rho, *eLight* **2022**, *2*, 1.
[31] Y. Zhao, R. Yang, W. Wan, X. Jing, T. Wen, S. Ye, *Chem. Eng. J.* **2020**, *389*, 124453.
[32] A. Nag, M. V. Kovalenko, J. S. Lee, W. Liu, B. Spokoyny, D. V. Talapin, *J. Am. Chem. Soc.* **2011**, *133*, 10612.
[33] Z. Wang, X. Yuan, L. Han, J. Li, X. Zhang, J. Hua, J. Wang, J. Zhao, H. Li, *J. Phys. Chem. C* **2022**, *126*, 3582.
[34] H. Luo, Y. Huang, H. Liu, B. Zhang, J. Song, *Chem. Eng. J.* **2022**, *430*, 132790.
[35] W. Cai, Z. Chen, Z. Li, L. Yan, D. Zhang, L. Liu, Q. H. Xu, Y. Ma, F. Huang, H. L. Yip, Y. Cao, *ACS Appl. Mater. Interfaces* **2018**, *10*, 42564.
[36] W. Zhu, W. Ma, Y. Su, Z. Chen, X. Chen, Y. Ma, L. Bai, W. Xiao, T. Liu, H. Zhu, X. Liu, H. Liu, X. Liu, Y. M. Yang, *Light: Sci. Appl.* **2020**, *9*, 112.
[37] R. Grisorio, E. Fanizza, I. Allegretta, D. Itamura, M. Striccoli, R. Terzano, C. Giannini, V. Vergaro, G. Ciccarella, N. Margiotta, G. P. Suranna, *Nanoscale* **2020**, *12*, 623.
[38] H. Moon, C. Lee, W. Lee, J. Kim, H. Chae, *Adv. Mater.* **2019**, *31*, 1804294.
[39] X. Pang, H. Zhang, L. Xie, T. Xuan, Y. Sun, S. Si, B. Jiang, W. Chen, J. Zhuang, C. Hu, Y. Liu, B. Lei, X. Zhang, *J. Mater. Chem. C* **2019**, *7*, 13139.
[40] S. Thapa, K. Bhardwaj, S. Basel, S. Pradhan, C. J. Eling, A. M. Adawi, J.-S. G. Bouillard, G. J. Stasiuk, P. Reiss, A. Pariyar, S. Tamang, *Nanoscale Adv.* **2019**, *1*, 3388.
[41] C. Carrillo-Carrion, S. Cardenas, B. M. Simonet, M. Valcarcel, *Chem. Commun.* **2009**, *35*, 5214.